Geo-Pol. Sci., Med. Geol. and Urban Geol. 2020 Vol.16, p.1-11
Article: Received 1 Aug. 2019; Accepted 7 Jan. 2020

Weathering processes of submarine hydrothermal deposits at the Hakurei site, Izena cauldron, Okinawa Trough

Haruka HATSUKAWA[1], Kazuo NAKASHIMA[2] and Takashi YUGUCHI [3]

1: Graduate School of Science and Engineering, Earth Sciences, Yamagata University, Yamagata 990-8560, Japan
2: ASN Co. Ltd., Sendai 989-3204, Japan
3: Department of Earth Sciences, Yamagata University, Yamagata 990-8560, Japan

Abstract

Two active hydrothermal vent sites, North and South mounds, from the Hakurei site were recently discovered in the Izena cauldron, Middle Okinawa Trough. Five samples from two mounds have been examined by microscope, X-ray diffraction and electron probe microanalyzer to evaluate the decomposition mechanism of submarine hydrothermal deposits. Regarding the primary minerals, barite, sphalerite, pyrrhotite, pyrite, galena and pyrargyrite have been found in the North mound samples, while barite, sphalerite, pyrite, galena, jordanite, geocronite and isocubanite are present in the South mound samples. The most remarkable difference between the two mounds is that pyrrhotite occurs in the North mound, whereas only pyrite exists as Fe-sulfide in the South mound. Pyrrhotite decomposes to Fe-hydroxides and native sulfur, and galena changes to anglesite in the North mound. On the other hand in the South mound, pyrite changes to only Fe-hydroxides, and galena changes to mimetite and cerussite.

The North mound is located on the flat bottom of the caldera where thick sediments pile up, resulting in highly reducing, and also in lowering pH, while the South mound is on the caldera slope where oxidation overwhelms on the weathering of this site. Finally all minerals and precipitates in ores exposed on the seafloor decompose in a few to tens of cm from the surface, and toxic elements such as As, Pb and Sb dissolve in seawater.

Keywords: Okinawa Trough, Izena cauldron, Hakurei site, hydrothermal deposit, weathering rind

Introduction

Submarine hydrothermal massive sulfide deposits are formed in mainly two types of tectonic environments; at the mid-ocean ridges (MOR) and at back-arc basins (BAB). The MOR type is large in general; for example, the TAG hydrothermally active mound is as large as 250 m wide and 50 m high (e.g., Rona and Speer, 1989) because the water depth is deep and resultant temperature of hydrothermal fluid is high. Since such MOR deposits are located away from continents and not covered by terrigenous sediments, most of them interact with oxidized seawater, resulting in dissolution and decomposition (weathering) on their surface. Weathering is defined in this paper as: a process whereby rocks and ores on the seafloor, when in contact with oxidized seawater, change their mineral composition due to oxidation, hydration, carbonatization, etc. On the other hand, the BAB type such as the Okinawa Trough are called sediment-hosted ridges and covered by thick terrigenous and pelagic to hemipelagic sediments (e.g., Sibuet et al., 1987) and the deposits are easily preserved as metal resources on a geologic timescale (Nakashima, 1996, 2006).

Mineralization type of the MOR deposits is simple and dominant in Cu and Zn (e.g., Rona, 1988), whereas that of the BAB deposits is a multi-element mineralization such as Zn, Pb, Sb, As, Ag and Au (e.g., Halbach et al. 1997). These differences are attributed to their tectonic settings and surrounding rocks/sediments because host rocks in the MOR are merely basalt, whereas those in the BAB are terrigenous and pelagic sediments and/or continental crust (Halbach et al., 1997). Since the mineralization types and tectonics of the BAB are similar to those of the Kuroko deposits of the Miocene Hokuroku district of Japan, the Okinawa Trough sulfide mineralization is thought to be a modern analogue of the Kuroko-type deposits (Halbach et al., 1989).

There are many papers and reports concerning mineralogical and chemical as well as biological and physical studies on submarine hydrothermal deposits (e.g., Lange, 1985), but few studies have been done on the weathering of the deposits (e.g., Thompson et al., 1988; Knott et al., 1998; Fallon et al, 2018). Understanding the weathering process of submarine hydrothermal deposits has great importance not only on mineral resources but on the flux of toxic metals and sulfur between the lithosphere and biosphere on the earth's surface. The aim of this study is to elucidate the weathering process and mechanism of submarine sulfide minerals using active chimney and mound samples from the Hakurei site, Izena cauldron, Okinawa Trough.

Tectonic setting and outline of sample location

The Okinawa Trough is a back-arc basin located behind the Ryukyu trench and Ryukyu Islands (Fig.1). The trough is about 1200 km long and 230 km wide, with a maximum water depth of about 2300 m (Letouzey and Kimura, 1986). Currently, seven hydrothermally active sites have been found (Kawagucci et al., 2010).

The Izena cauldron is located in the Middle Okinawa Trough and

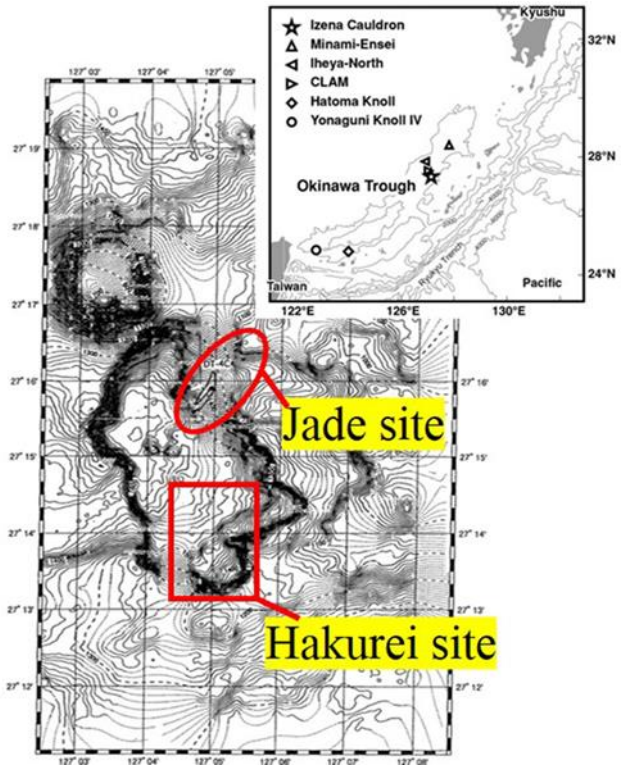

Fig.1 Location of the Izena cauldron and two hydrothermal sites, Jade and Hakurei, in the cauldron (modified after Kawagucci et al., 2010; Glasby and Notsu, 2003).

has a rectangular shape of 6 x 3 km, and a maximum depth of 1,665m. There are two large hydrothermal fields in the Izena cauldron, Jade and Hakurei sites. The Jade site is located on the inside slope of the north-eastern wall of the Izena cauldron at a water depth of 1,550–1,300 m (Fig. 1). Hydrothermal activity, up to 320 °C, was recognized in an area of 500 × 300 m. The Hakurei site is located on the southern bottom to foot of the depression of the Izena cauldron, at water depths of 1,600–1,630 m (Fig. 2). This site has been explored intensively by JOGMEC (Japan Oil, Gas and Metals National Corporation) under the framework of the ocean energy and mineral resources development program since 2008, and Zn-rich polymetallic sulfide mineralization was extensively recognized (METI, 2013). Geological and geochemical features are well summarized by Kawagucci et al. (2010) and Ishibashi et al. (2014). Based on recent seismological observations during the R/V Kaiyo KY02-11 cruise, the Hakurei site is covered by a sediment layer over 150 m in thickness (Kawagucci et al., 2010). Sediments in the cauldron comprise tuff, tuff breccia, tabular-jointed pumice and mud (Kato et al., 1989).

Sample and methods

Samples used in this study were collected by the Hakurei-maru, during the No. 5 Survey Cruise of JOGMEC, in August 2013. There are two hydrothermal mounds at the Hakurei site, the North and South mounds. The South mound is located on the slope of the caldera wall and only thin sediments are deposited, while the North mound is on the bottom of the caldera where a thick sediment pile has accumulated.

In this study, we selected five samples which have a remarkable weathered appearance and also have many types of minerals; two, FPG 10-2 and FPG 12, from the North mound, and three, FPG 03, ROV01-1 and FPG 08-2 from the South mound.

Mineral compositions were deteremined by wavelength-dispersive electron probe microanalyzer, JEOL JXA 8900, at the Earth Science Lab. in Yamagata University. Accelaretion voltage and beam current were set to 20 kV and 20 nA, respectively. The weathered rinds (red brownish and rusted surface) of samples were also examined by XRD, RIGAKU Mini Flex II.

Results

Minerals and weathered products observed in each mound are summarized as Table 1. Barite and sulfide minerals are formed earlier in the hydrothermal stage, and so are referred to as primary minerals while sulfates, carbonates and arsenate are identified as secondary minerals, and hydroxide and amorphous phases are as weathering products. Mineral occurrences in each sample are summarized in Table 2. Since identification of the real phase name is difficult for some hydroxides and sulfates, the following criteria are made for convenience; Fe-hydroxides are FeO > 30 wt.% and SO_3 < 10 wt.%, Fe-sulfates are FeO > 20 wt.% and SO_3 > 10 wt. %, and Fe-silicates are SiO_2 > 30 wt.% and containing FeO in some amounts (Tables 3, 4).

Weathering process in the North mound

Sample FPG 10-2 is a dark and porous ore. The weathered rind is brownish orange in color and 1-5 mm in thickness (Fig. 3a, b). This sample consists of pyrrhotite, barite, sphalerite and galena as the primary minerals. Sample FPG 12 has a weathered rind that is ocher-brown in color and 1-2 mm in thickness (Fig. 3c, d) and includes pyrrhotite, barite, sphalerite, galena and pyrargyrite as the primary minerals.

Fe-sulfide: In the North mound, it is striking that pyrrhotite exists as a Fe-sulfide in addition to pyrite. The pyrrhotite has been broken up along its cleavage and it remains as a stripe (Fig. 4a). In such altered pyrrhotite, native sulfur has been often precipitated as well as Fe-hydroxides (Fig. 4b, c).

Sulfosalts (Pyrargyrite): pyrargyrite is present in some sphalerite crystals in FPG 12. There are no secondary minerals and weathering products including Ag and Sb around this mineral (Fig. 4f).

Barite and Sphalerite: There are no weathering products including Ba and Zn around barite and sphalerite. In the weathered rind, most of these minerals have dissolved and Fe-hydroxides and Fe-sulfates have precipitated around these minerals (Fig. 4g).

Galena: Anglesite is frequently observed around galena (Fig. 4h). This means that anglesite has formed after galena, in later oxidized conditions.

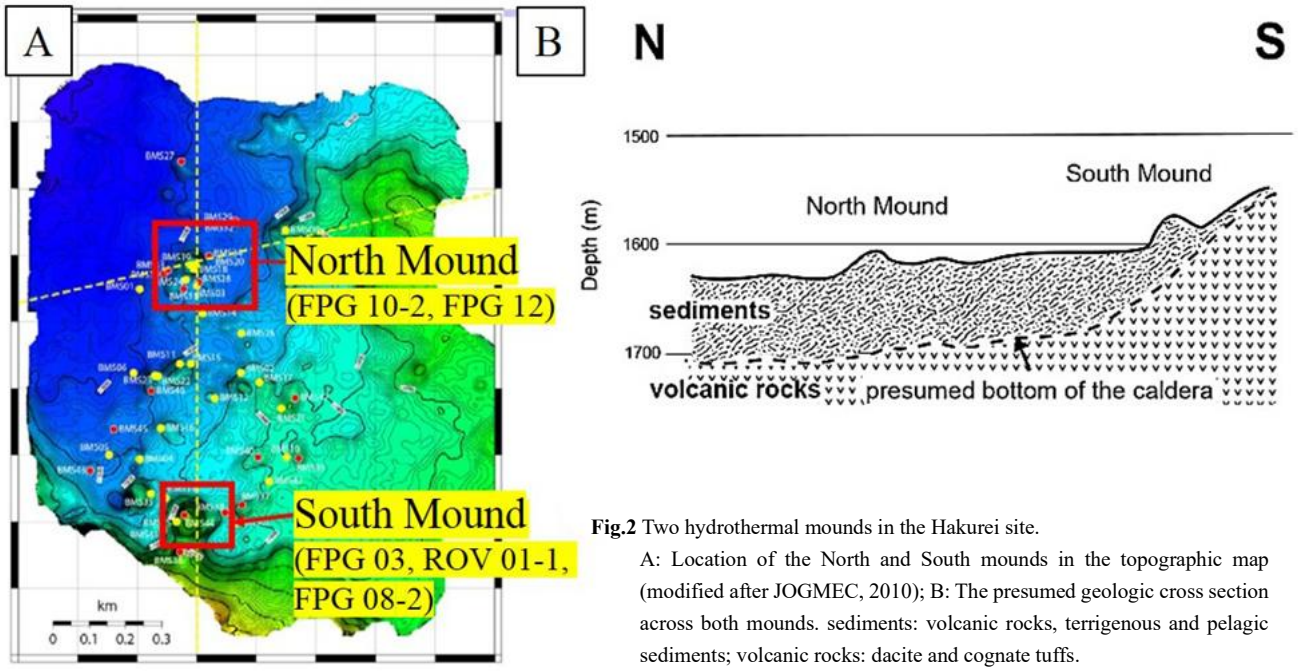

Fig.2 Two hydrothermal mounds in the Hakurei site.
A: Location of the North and South mounds in the topographic map (modified after JOGMEC, 2010); B: The presumed geologic cross section across both mounds. sediments: volcanic rocks, terrigenous and pelagic sediments; volcanic rocks: dacite and cognate tuffs.

Table 1 The abbreviations and composition of each mineral observed in this study

Minerals		Abbreviations	Compositions
Primary Minerals	Barite	Ba	$BaSO_4$
	Sphalerite	Sph	(Zn, Fe) S
	Pyrite	Py	FeS_2
	Pyrrhotite	Po	Fe_7S_8
	Jordanite	Jo	$Pb_{14}(As, Sb)_6S_{23}$
	Geocronite	Ge	$Pb_{14}(Sb,As)_6S_{23}$
	Galena	Gl	PbS
	Isocubanite	Icu	$CuFe_2S_3$
	Pyrargyrite	Pyr	Ag_3SbS_3
Secondary Minerals・Weathering Products	Anglesite	Ang	$PbSO_4$
	Mimetite	Mim	$Pb_5(AsO_4)_3Cl$
	Cerussite	Cer	$PbCO_3$
	Amorphous silica	Ams	SiO_2
	Fe-hydroxide	Fe-hy	FeOOH
	Fe-sulfates	Fe-sul	($FeSO_4$)
	Fe-silicates	Fe-Si	($Fe+SiO_2$)
	Native sulfur	Sul	S

Table 2 Mineral assemblages of each sample.

Minerals		North Mound		South Mound		
		FPG 10-2	FPG 12	FPG03	ROV 01-1	FPG 08-2
Primary Minerals	Barite	✓	✓	✓	✓	
	Sphalerite	✓	✓		✓	✓
	Pyrite	✓		✓		✓
	Pyrrhotite		✓			
	Jordanite				✓	
	Geocronite				✓	
	Galena	✓	✓		✓	
	Isocubanite					✓
	Pyrargyrite		✓			
Secondary Minerals・Weathering Products	Anglesite	✓	✓		✓	✓
	Mimetite				✓	
	Cerussite				✓	
	Amorphous silica				✓	
	Fe-hydroxide	✓	✓	✓		✓
	Fe-sulfates		✓	✓		✓
	Fe-silicates			✓		✓
	Native sulfur		✓			

Table 3 Representative analytical results of chemical composition of primary minerals (in wt. %)

Element	Sphalerite		Pyrite		Pyrrhotite	Jordanite	Geocronite	Galena		Isocubanite	Pyrargyrite
	N	S	N	S	N	S	S	N	S	S	N
As	n.d.	0.09	0.02	0.25	n.d.	9.45	5.62	n.d.	0.36	n.d.	1.71
Sb	n.d.	0.02	n.d.	n.d.	n.d.	0.07	0.31	0.03	0.05	n.d.	18.64
Zn	46.12	64.34	n.d.	0.09	n.d.	n.d.	0.65	0.32	0.73	2.85	0.04
S	33.79	33.48	53.16	52.72	38.98	17.92	17.01	13.03	13.85	35.29	17.79
Fe	19.35	2.59	47.03	46.97	59.54	0.05	n.d.	0.15	0.02	40.09	0.36
Ag	n.d.	0.01	0.09	0.03	0.03	n.d.	n.d.	n.d.	n.d.	0.07	60.68
Mn	0.11	0.01	0.02	0.05	n.d.	n.d.	0.03	n.d.	n.d.	0.02	n.d.
Pb	0.18	0.22	0.16	0.51	0.30	69.45	67.85	86.41	85.48	n.d.	0.07
Cu	0.31	0.57	0.01	0.01	n.d.	n.d.	0.03	0.05	0.04	20.30	0.10
Cd	n.d.	n.d.	n.d.	n.d.	n.d.	0.09	0.01	n.d.	n.d.	n.d.	n.d.
Hg	n.d.	n.d.	n.d.	n.d.	0.15	n.d.	0.12	n.d.	n.d.	0.05	0.13
Total	99.86	101.33	100.49	100.64	99.01	97.02	91.65	99.99	100.53	98.68	99.52

n.d.: not detected

Table 4 Representative analytical results of chemical composition of secondary minerals and weathering products (in wt. %)

Metal Oxides	Anglesite		Mimetite	Cerussite	Amorphous Silica	Fe-hydroxides		Fe-sulfates		Fe-silicates
	N	S	S	S	S	N	S	N	S	S
SiO_2	n.d.	0.08	0.08	n.d.	47.48	0.11	1.10	0.01	0.28	38.56
Al_2O_3	0.01	0.13	n.d.	n.d.	n.d.	n.d.	0.01	0.02	n.d.	0.02
TiO_2	n.d.	n.d.	n.d.	0.04	n.d.	n.d.	n.d.	0.03	0.02	n.d.
FeO	0.34	0.75	0.08	0.05	7.29	34.23	37.91	20.08	28.69	15.44
Na_2O	n.d.	0.03	0.66	0.02	n.d.	0.25	0.17	3.25	1.13	1.34
MnO	0.06	0.02	n.d.	n.d.	n.d.	0.12	0.03	0.07	0.07	0.08
P_2O_5	n.d.	n.d.	0.04	n.d.	0.14	n.d.	0.20	0.03	0.20	0.29
K_2O	0.12	0.05	0.13	0.05	0.04	0.05	0.06	1.53	0.02	0.20
CuO	n.d.	0.22	0.38	0.04	0.24	0.08	n.d.	0.01	0.03	n.d.
As_2O_5	n.d.	n.d.	15.14	n.d.	0.54	2.67	2.96	n.d.	3.52	0.44
Cl	0.13	3.34	2.95	1.40	1.29	0.21	1.14	0.08	1.47	0.08
Cr_2O_3	n.d.	0.02	n.d.	0.03	0.02	0.02	n.d.	n.d.	n.d.	0.01
SO_3	24.01	22.34	2.37	n.d.	4.97	4.69	5.05	25.57	21.33	8.52
ZnO	0.12	1.31	0.06	0.03	26.61	1.63	0.41	0.25	0.03	0.34
PbO	71.94	68.14	76.23	83.24	0.85	0.20	0.04	4.93	0.46	0.83
Bi_2O_3	3.81	2.30	1.76	1.00	1.30	2.04	n.d.	0.98	n.d.	2.69
Sb_2O_5	n.d.	0.01	0.06	n.d.	1.04	0.23	0.33	0.21	0.32	0.22
BaO	0.55	n.d.	n.d.	0.13	0.05	n.d.	0.01	n.d.	0.30	n.d.
Total	101.14	98.04	99.33	85.81	92.08	46.47	49.63	57.08	57.72	69.13

n.d.: not detected

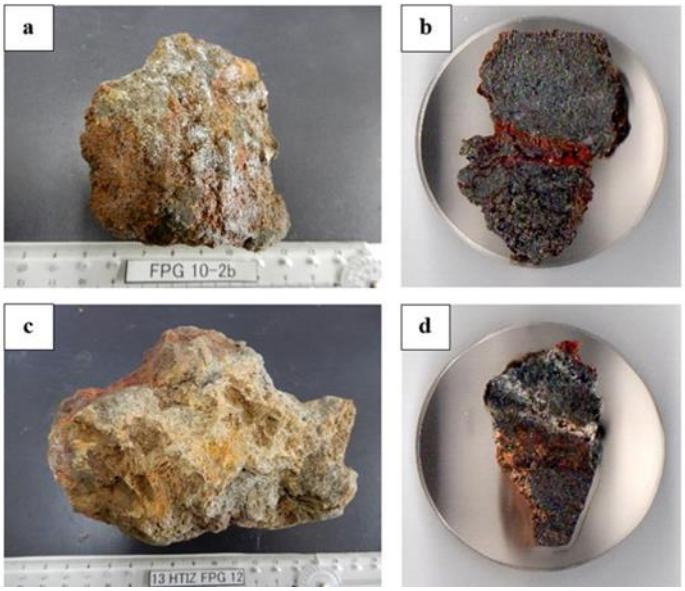

Fig.3 Photographs of ores and cut sections of the North mound samples.
a, b (FPG10-2): Brownish to orangish weathered rind develops on the surface, and white small needle-like aggregates have crystallized on most of the surface which were formed in the air after collection and identified as rozenite ($FeSO_4 \cdot 4H_2O$) by XRD (Fig. 3a); Reddish rust zone develops along inner porous part of the ore (Fig. 3b); c, d: Ocher-brownish weathered rind covers the surface (Fig. 3c), and white products, mostly amorphous silica, precipitate around pores arranged in lines, and a reddish and brownish zone develops in the inner parts (Fig. 3d).

Weathering process in the South Mound

The sample FPG 03 is a gray-colored ore which consists of pyrite and barite, and ocher and powdery weathered rind develops characteristically on the surface (Fig. 5a, b). Sample ROV 01-1 is a dark colored and porous ore which consists mainly of barite and sphalerite, and galena, jordanite and geocronite in minor amounts as primary minerals, and a weathered rind of 1-5 mm in thickness develops from the surface to inner part (Fig. 5c, d). In sample FPG 08-2, red to brown colored weathered rind has been observed (Fig. 5e, f), and it contains sphalerite, pyrite, galena and isocubanite. White-colored crystals observed on the surface are also rozenite which was formed after collection in the air.

Fe-sulfides: Pyrite is the sole Fe-sulfide in the South mound. The pyrite changes to Fe-hydroxides and Fe-sulfates (Fig. 6a, b). Fe-silicates precipitate on the surface of the heavily weathered part. In some cases, there are two layers on the barite crystals, Fe-hydroxides and Fe-sulfates with the former as the innermost layer (Fig. 6c-e).

Sulfosalts (jordanite and geocronite): Jordanite is a solid solution with geocronite and these minerals are closely associated with each other (Fig. 6g). Mimetite, a secondary Pb-As oxide mineral, precipitates on the eroded and rounded surface of jordanite (Fig. 6g). In heavily weathered parts, galena and jordanite decompose and only mimetite remains (Fig. 6h).

Barite and sphalerite: Barite and sphalerite dissolve in the weathered rind and there is no Ba- or Zn-bearing secondary minerals.

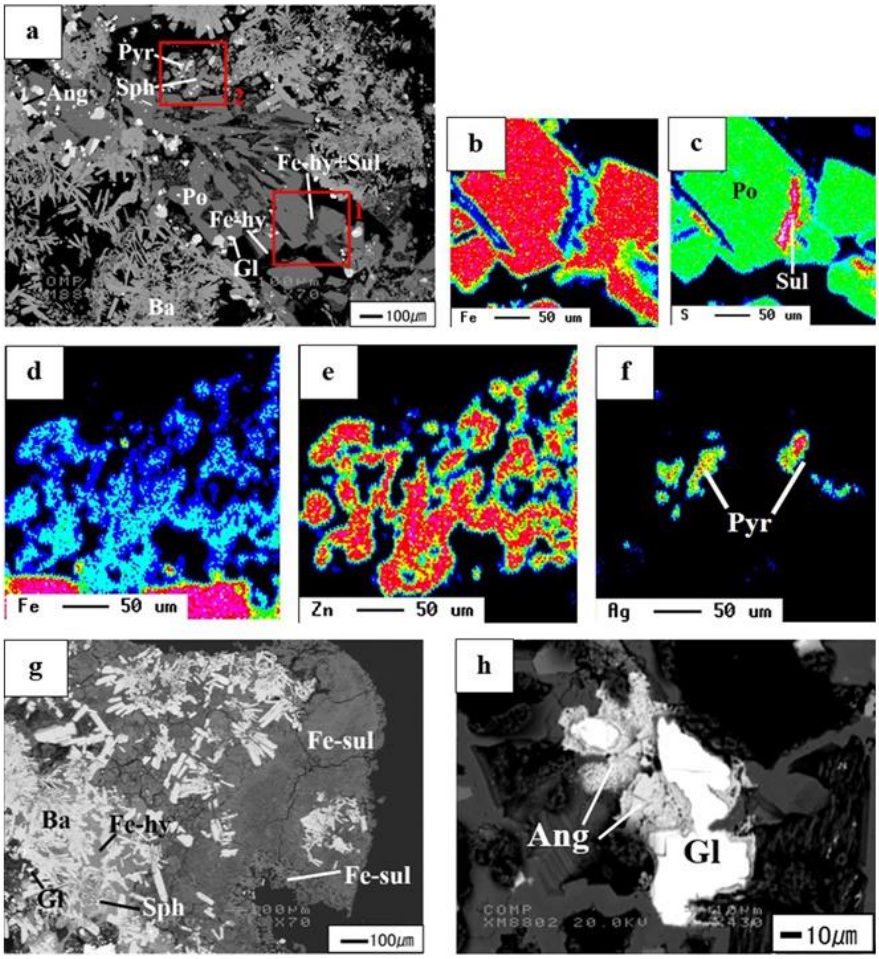

Fig.4 BSE (Back-scattered electron) images and elemental mappings of the North mound samples.
a (FPG 12): BSE image showing alteration of pyrrhotite; b-c: Elemental mappings of Fe (b) and S (c) of the square 1 in (a) showing an occurrence of native sulfur; d-f: Elemental mappings of Fe (d), Zn (e) and Ag (f) of the square 2 in (a) showing pyrargyrite in sphalerite; g: Weathered rind of FPG 12 showing barite and sphalerite decompose and Fe-hydroxides and Fe-sulfates precipitate around them; h: Anglesite is formed around galena (FPG 10-2)

Amorphous silica including Zn, Fe and Cl in some amounts (Table 4) precipitates in these altered parts. Sphalerite dissolves at the boundary between the fresh ore part and weathered rind, and Fe-hydroxides and Fe-sulfates precipitate around sphalerite (Figs. 6b, 7d and 7e).

Galena: Anglesite frequently surrounds galena which often accompanies mimetite and cerussite as secondary Pb-bearing minerals (Fig. 6f, g, i). Galena is also rounded and contacts with jordanite and mimetite precipitated on the surface of these minerals (Fig. 6f, g). Cerussite precipitates in contact with mimetite or among mineral grains interstitially.

Cu-bearing sulfide: Isocubanite, the sole Cu-bearing sulfide in this site, occurs in sphalerite with a diseased texture (Fig. 7e), and there is no secondary Cu-bearing phase in the weathered rind.

Mineral sequence

Based on our observation, a sequence of mineral formation and precipitation was obtained (Fig. 8). Three major stages are observed in both mounds: hydrothermal, retrograde and weathering stages. During the hydrothermal stage primary sulfide minerals precipitate at an elevated temperature; during the retrograde stage sulfate and carbonate mineral replacement occurs after sulfide minerals in a moderate to lower temperature hydrothermal solution mixed with seawater; during the weathering stage hydroxides and amorphous phases precipitate in the seawater (Fig. 8A). These sequences are based on the following observations; sphalerite decomposed and Fe-hydroxides and Fe-sulfates precipitated around sphalerite and pyrite (Fig. 6a-c); anglesite (in both mounds) and mimetite and cerussite (in the South mound) formed around galena; amorphous silica and Fe-hydroxides precipitated in most of the weathered rinds (Fig. 7a, d). Around the primary sulfide, sulfates, carbonates and oxides of the retrograde stage were formed next, and then weathering precipitates as shown by the lower total of EPMA analyses were formed finally.

Discussions

Mineral change during weathering

Fe-S minerals: There are pyrite and pyrrhotite in the North mound but only pyrite in the South mound. In the weathered rind of ores studied, pyrite changed to Fe-hydroxides and Fe-sulfates, whereas pyrrhotite changed to Fe-hydroxides, Fe-sulfates and native sulfur (Figs. 4a, 6a). The XRD measurements revealed that the brownish to reddish outer rind is mainly composed of goethite and lepidocrocite, both are Fe-hydroxides.

These differences are based on the degree of oxidation; at elevated temperatures, pyrrhotite precipitate easily under a reductive

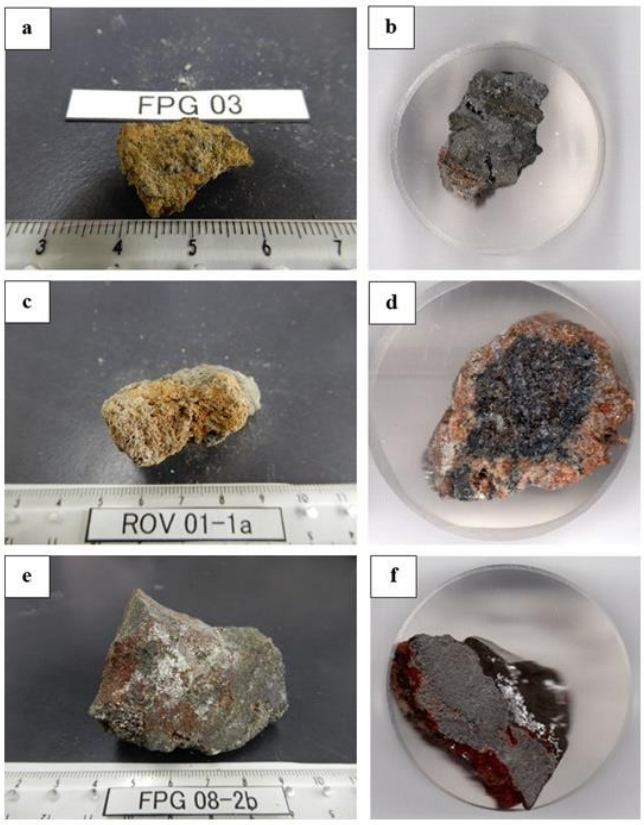

Fig.5 Photographs of ores and cut sections of the South mound sample. a, b (FPG 03) Sample surface changes to ocher-colored and powdered weathered rind; c, d: A thick red brownish weathered rind surrounds the sample; e, f: A thin reddish weathered film develops on the surface (e), and secondary white needles of rozenite develop along cracks (f).

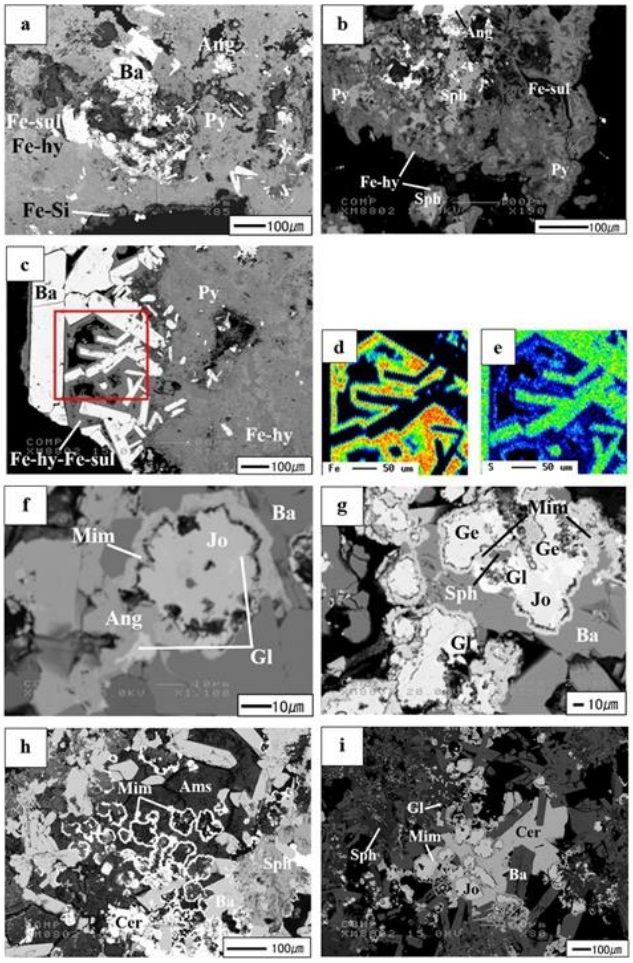

Fig.6 BSE images and elemental mappings of the South mound samples.

a (FPG 03): Decomposition of barite and pyrite, and Fe-hydroxides, Fe-sulfates and Fe-silicates precipitate in the surroundings; b (FPG 08-2): Break down of sphalerite and pyrite, and Fe-hydroxides and Fe-sulfates precipitate around them; c-e (FPG 03): two layers of Fe-hydroxides and Fe-sulfates precipitate on the barite surface with the former as the innermost layer; f (ROV 01-1): Intimate association of galena and jordanite is covered by anglesite and mimetite; g (ROV 01-1) Jordanite and geocronite, a solid solution of As-Sb substitute, is covered by mimetite; h (ROV 01-1): Galena or jordanite perfectly dissolved and ring-shaped mimetite remains; i (ROV 01-1): Cerussite fills cavity and contacts with mimetite and jordanite.

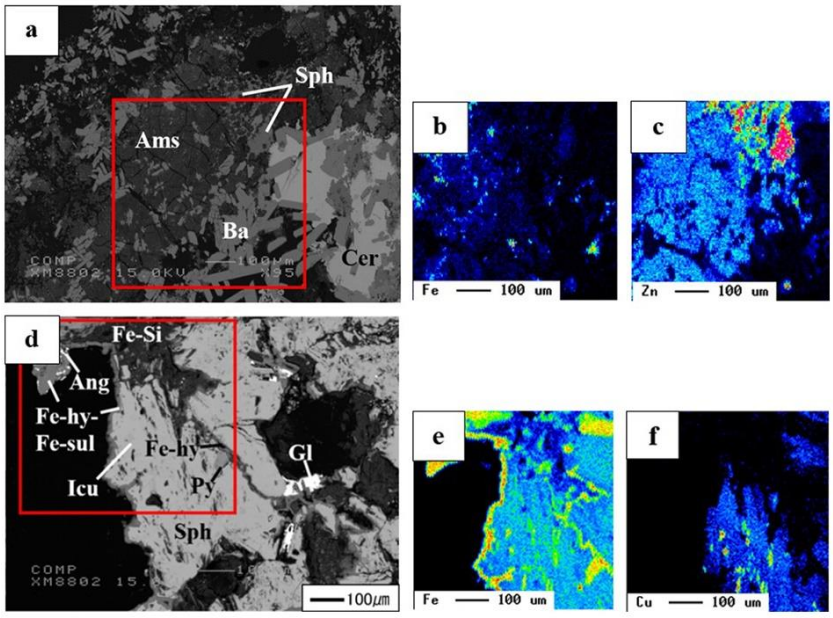

Fig.7 BSE images and elemental mappings of the South mound samples (Continued).
a (ROV 01-1): Amorphous silica precipitates in the space where barite and sphalerite dissolved. Cerussite precipitates in mineral spaces; b, c: Amorphous silica contains Zn, Fe and Cl; d: (FPG 08-2): Fe-hydroxides and Fe-sulfates precipitate on the surface of sphalerite, and Fe-silicates precipitate among them; e, f: Sphalerite includes isocubanite in a diseased texture.

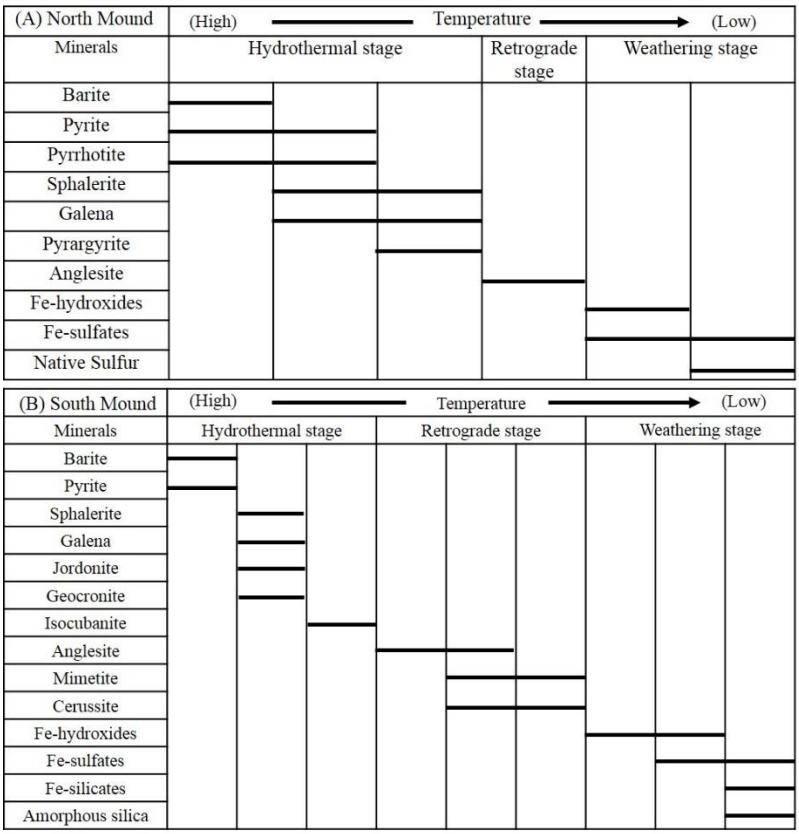

Fig.8 Paragenetic sequence in mineral formation of the North mound (A) and the South mound (B).

condition than pyrite (e.g., Cooke et al., 2000; Hanor, 2002). This condition is inherited to low temperatures as shown in Figure 9A; pyrrhotite (FeS) is stable at lower Eh than pyrite (FeS_2). This means that the North mound is relatively reductive and the South mound is oxidized.

Pyrrhotite in the North mound changed to Fe-hydroxides and native sulfur. This is caused by a large pH decrease (Fig. 9A). Pyrite changed to Fe-hydroxides, and this is caused mainly by oxidation influenced by seawater. These changes in pyrrhotite and pyrite are expressed by the following reactions (1) and (2), respectively (Nesbitt and Jambor, 1988).

$$Fe_7S_8 + 4H_2O + 5O_2 \rightarrow 7FeOOH + H^+ + 8S + e^- \quad (1)$$
pyrrhotite Fe-hydroxide native sulfur

$$FeS_2 + 2.5H_2O + 3.25O_2 \rightarrow FeOOH + 4H^+ + 2SO_4^{2-} \quad (2)$$
pyrite Fe-hydroxide

Sphalerite: Sphalerite is a solid solution between ZnS and FeS. Fe-content in sphalerite in the North mound is higher (av. 16.7 mol.%, n = 17) than in the South mound (av. 4.5 mol.%, n = 21) (Table 3). Fe-content in sphalerite changed mainly in accordance with the sulfur fugacity of hydrothermal fluids (e.g., Scott and Barnes, 1971), and this is nearly equal to the oxidation state; Fe-enrichment is the reduced and Fe-scarcity is the oxidized condition. This means that the North mound is more reducing than the South mound.

In outer brownish rind of ore samples in both mounds, sphalerite dissolved and Fe-hydroxides precipitated around sphalerite. This dissolution of sphalerite and precipitation of Fe-hydroxides is expressed in the following reaction (3). In this reaction, sphalerite composition has been assumed to be ZnS : FeS = 0.9 : 0.1 (in mole).

$$(Zn_{0.9}, Fe_{0.1})\,S + 0.915H_2O + 1.575O_2$$
sphalerite $$\rightarrow 0.9Zn^{2+} + 0.1FeOOH + 2H^+ + SO_4^{2-} \quad (3)$$
Fe-hydroxide

Sphalerite does not form a secondary Zn-bearing mineral, and it may have dissolved in reaction with the oxidized seawater (Fig. 9B). Amorphous silica in the weathered rind includes Zn, Fe and Cl, and this is caused by dissolution of sphalerite and Fe-minerals in the vicinity.

Galena: Anglesite (in both mounds), mimetite and cerussite (in the South mound) occur around galena in the weathered rind. In the Eh-pH diagram, a large decrease of pH leads to a change from galena to anglesite in the North mound (Fig. 9C), whereas the oxidation of galena in the South mound results in anglesite or cerussite in three ways: galena to anglesite (arrow A in Fig. 9C; reaction 4; Younger et al., 2002), galena through anglesite to cerussite (reaction 5, Hideshima et al., 2013), and galena to cerussite (reaction 6; arrow B in Fig. 9C). In the South mound, mimetite has Cl in the crystal structure and cerussite includes Cl in 1 - 2 wt.% (Table 4). Therefore, the South mound is affected by seawater more than the North mound, and the reaction proceeded near the Eh and pH conditions of seawater.

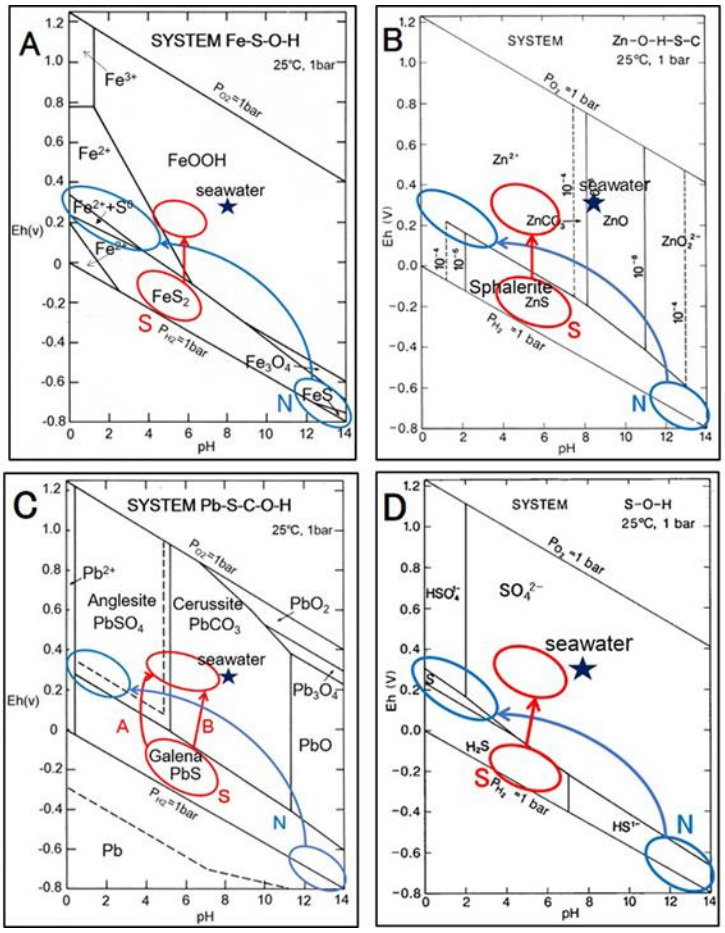

Fig.9 Eh-pH diagrams (modified after Brookins, 1988). A: Fe-S-O-H system (Fe=10^{-6}, S=10^{-3} M), pyrrhotite is shown as FeS, and pyrite is FeS, B: Zn-O-H-S-C system (Zn=$10^{-6,-4}$, C=10^{-3}, S=10^{-3}) C: Pb-S-C-O-H system (Pb=$10^{-6,-8}$, S=10^{-3}, C=10^{-3}) D: S-O-H system (S=10^{-3} M)

$PbS + 2O_2 \rightarrow PbSO_4$ (4)
galena anglesite

$PbSO_4 + HCO_3^- = PbCO_3 + SO_4^{2-} + H^+$ (5)
anglesite cerussite

$PbS + HCO_3^- + 4H_2O = PbCO_3 + SO_4^{2-} + 9H^+ + 7e^-$ (6)
galena cerussite

As-Sb sulfosalts: Since the secondary minerals of jordanite, geocronite, isocubanite and pyrargyrite have never been seen in the studied samples, these minerals finally dissolve under heavy weathering. Therefore, toxic elements such as Pb, As and Sb would have dissolved in seawater.

Barite: The solubility of barite in a hydrothermal solution reaches a peak near 100 °C (Blount, 1977), therefore, barite dissolves under slightly high temperature, at the retrograde stage of hydrothermal mineralization (reaction 7). Ba dissolves in seawater, while S also dissolves in seawater or is used to make secondary sulfides or sulfosalts.

$BaSO_4 \rightarrow Ba^{2+} + SO_4^{2-}$ (7)
barite

Fe-hydroxides: There are several Fe-hydroxide phases in the studied sample, and they are sometimes arranged into colloform or banded texture (Fig. 6c-e). Since Fe content in these banded layers decreases and S content increases outward, Fe in Fe-hydroxides dissolved in seawater, and the phases finally decomposed.

Weathering environments of both mound sites

Weathering environments of both sites are different even in the same caldera; the North is reductive and the South is oxidative. Moreover, the North mound has a low pH, whereas in the South mound it is higher and much affected by seawater (Fig. 9D). These differences are explained as follows.

As described above, the North mound is located on the flat bottom of the caldera and the mound occurs on a thick sediment pile of about 150 m in thickness (Kawagucci et al., 2010), whereas the South mound is located near the caldera slope and the thickness of the surrounding sediments is thinner (Fig. 2B). In these sediments in the Okinawa Trough, there is much organic matter, and this leads to a reductive environment (e.g., Gamo et al., 1991) The cause of low pH in the North mound is as follows; the reductive environment leads to much H_2 in the ambience and a part of H_2 dissociates into H^+ (reaction 8), and this causes high acidity.

$H_2 = 2H^+ + 2e^-$ (8)

Table 5 Summary of formation and dissolution of minerals observed in this study.

Primary mineral	Sequence of decomposition	
	North Mound	South Mound
Fe-sulfides	Pyrrhotite → Fe-hydroxides, Native sulfur Pyrite → Fe-hydroxides	Pyrite → Fe-hydroxides
Sphalerite	Fe-hydroxides	Fe-hydroxides
Galena	Anglesite	Anglesite → Mimettite, Cerussite
Barite	dissolved	dissolved
Pyrargyrite	dissolved	-
Jordanite	-	dissolved
Geocronite	-	dissolved
Isocubanite	-	dissolved

In the North mound, native sulfur occurs after pyrrhotite. This may have been formed by abundant H_2 and H^+, resulting in a lowering of pH as the native sulfur formed (Fig. 9D).

As described above, the difference in oxidation state at both sites leads to different secondary minerals and weathering products, and this is caused by a difference in the geologic setting and special location in the caldera.

Summary and conclusion

The weathering mechanism of submarine hydrothermal ores from the Hakurei site, Izena Cauldron, Okinawa Trough, has been examined mineralogically, and the following results were obtained. The results are summarized in Table 5.

1. For Fe-sulfide minerals, pyrrhotite occurs in the North mound, whereas only pyrite was observed in the South mound. This is in harmony with the occurrence of Fe-rich sphalerite in the North mound. These characters indicate that the North mound is more reducing than the South mound.

2. Pyrrhotite in the North mound changed to Fe-hydroxides and native sulfur, whereas pyrite in the South mound changed only to Fe-hydroxides. Since native sulfur is stable only in a very low pH condition, primary sulfides in the North mound have decomposed in a high acidity environment.

3. Galena changed only to anglesite in the North mound, whereas it changed to mimetite and cerussite in addition to anglesite in the South mound. These facts indicate that pH is higher and more oxidized in the South mound than the North mound.

4. There are no weathering products on barite in both mounds, pyrargyrite in the North mound, jordanite, geocronite and isocubanite in the South mound. These minerals dissolved directly in seawater not through weathering products. In the weathering rind, final precipitates are Fe-hyroxides, amorphous silica including Zn, Pb, Bi, As and Cl and Fe-silicates, but these precipitates may finally decompose and toxic elements such as Pb, As and Sb dissolved in seawater.

5. The North mound is located on the flat bottom of the caldera, and thick sediments lead to reduction and pH decreases by the dissociation of H_2. On the contrary, the South mound is located on the slope of the caldera, and the thickness of sediments is thinner. This leads to a more oxidized condition than in the North mound, and weathering proceeded near the pH-Eh conditions of seawater.

Acknowledgements: We wish to express sincere gratitude to Keita Koda, JOGMEC, for providing us ore samples, Yuya Izumino, Yamagata University, for assistance in mineral identification, R.W. Jordan of Yamagata University for improving the English in this manuscript. We also thank Osamu Kazaoka for his editorial handling, and Yoshikaki Tainosho and an anonymous reviewer for their insightful comments.

References

Blount, C.W., 1977, Barite solubilities and themodynamic quantities up to 300 °C and 1400 bars. *American Mineralogist*, vol. 62, 942-957.

Brookins, D. G., 1988, Eh-pH Diagrams for Geochemistry. Springer-Verlag, 176p.

Cooke, D.R., Bull, S.W., Large, R.R. and McGoldrick, P.J., 2000, The importance of oxidized brines for the formation of Australian Proterozoic stratiform sediment-hosted Pb-Zn (Sedex) deposits. *Economic Geology*, vol. 95, 1-18.

Fallon, E. K., Niehorster, E., Brooker, R. A. and Scott, T. B., 2018, Experimental leaching of massive sulphide from TAG active hydrothermal mound and implications for seafloor mining. *Marine Pollution Bulletin*, vol. 126, 501-515.

Gamo, T., Sakai, H., Kim, E-S., Shitashima, K. and Ishibashi, J., 1991, High alkalinity due to sulfate reduction in the CLAM

hydrothermal field, Okinawa Trough. *Earth and Planetary Science Letters*, vol. 107, 328-338.

Glasby, G. P. and Notsu, K., 2003, Submarine hydrothermal mineralization in the Okinawa Trough, SW of Japan: an overview. *Ore Geology Review*, vol. 23, 299-339.

Halbach, P., Hansmann, W., Koppel, V. and Pracejus, B., 1997, Whole-rock and sulfide lead-isotope data from the hydrothermal JADEW field in the Okinawa back-arc trough. *Mineralium Deposita*, vol. 32, 70-78.

Halbach, P., Nakamura, K., Wahsner, M., Lange, J., Sakai, H., Käselitz, L., Hansen, R.-D., Yamano, M., Post, J., Prause, B., Seifert, R., Michaelis, W., Teichmann, F., Kinoshita, M., Märten, A., Ishibashi, J., Czerwinski, S. and Blum, N., 1989, Probable modern analogue of Kuroko-type massive sulphide deposits in the Okinawa Trough back-arc basin. *Nature*, vol. 338, 496-499.

Hanor, J. S., 2002, Barite-celestine geochemistry and environments of formation. *In Alpers, C. N., Jambor, J. L., Nordstrom, D. K. eds. Sulfate Minerals, Reviews in Mineralogy & Geochemistry, Reviews in Mineralogy & Geochemistry*, Mineralogical Society of America and Geochemical Society, vol. 40, 193-275.

Hideshima, Y., Nakata, M. and Komuro, K., 2013, Formation of cerussite from anglesite: an experimental approach with sodium bicarbonate solution. *Resource Geology*, vol. 63, 143-147. *

Ishibashi, J., Ikegami, F., Tsuji, T. and Urabe, T., 2014, Hydrothermal activity in the Okinawa Trough back-arc basin: geological background and hydrothermal mineralization. *In Ishibashi et al. eds. Subseafloor Biosphere Linked to Hydrothermal Systems, TAIGA Concept*, 337-359, Open Access, Springer Nature, 656 p.

JOGMEC, 2010, Exploration of resource quantity of submarine hydrothermal deposits and examination of mineral processing and refining, 34p. **

Kato, Y., Nakamura, K., Iwabuchi, Y., Hashimato, J. and Kaneko, Y., 1989, Geology and topography in the Izena Hole of the Middle Okinawa Trough - the results of diving surveys in 1987 and 1988 -. *JAMSTEC DEEPSEA RESEARCH*, 163-182. *

Kawagucci, S., Shirai, K., Lan, T. F., Takahata, N., Tsunogai, U., Sano, Y. and Gamo, T., 2010, Gas geochemical characteristics of hydrothermal plumes at the HAKUREI and JADE vent sites, the Izena Cauldron, Okinawa Trough. *Geochemical Journal*, vol. 44, 507 - 518.

Knott, R., Fouquet, Y., Honnorez, J., Petersen, S. and Bohn, M., 1998, 1. Petrology of hydrothermal mineralization: a vertical section through the TAG mound. *in Herizig et al. eds. Proceedings of the Ocean Drilling Program, Scientific Results*, vol. 158, 5-26.

Lange, J. A., 1985, Abstract in Pacific Marine Mineral Resources Training Course, Honolulu, 13-21.

Letouzey, J. and Kimura, M., 1986, The Okinawa Trough: genesis of a backarc basin developing along a continental margin. *Tectonophysics*, vol. 125, 209-230.

METI, 2013, Report for the first stage of the program. Development of deep-sea mineral resources. http://www.meti.go.jp/press/2013/07/20130705003/20130705003-2.pdf **（accessed on 16 May 2019）

Nakashima, K., 1996, Submarine hydrothermal deposits in back-arc basins. *Gekkan Chikyu*, no. 16, 49-54. **

Nakashima, K., 2006, Present situation on exploration of submarine hydrothermal deposits. *Yamagata Oyo Chishitu*, no. 26, 1-6. **

Nesbitt, H. W. and Jambor, J. L., 1988, Role of mafic minerals in neutralizing and, demonstrated using a chemical weathering methodology. *In L. J. Cabri and D. J. Vanghan eds. Modern Approaches to Ore and Environmental Mineralogy*, MAC Short Course Series, no. 27, 403-421.

Rona, A., 1988, Hydrothermal mineralization at oceanic ridges. *Canadian Mineralogist*, vol. 26, 431-465.

Rona, A. and Speer, K.G., 1989, An Atlantic hydrothermal plume: Trans-Atlantic geotraverse (TAG) area, Mid-Atlantic Ridge crest near 26°N. *Journal of Geophysical Research (Solid Earth)*, vol. 94, 13879-13893.

Scott, S.D. and Barnes, H.L., 1971, Sphalerite geothermometry and geobarometry. *Economic Geology*, vol. 66, 653-669.

Sibuet, J.-C., Letouzey, J., Barbier, F., Charvet, J., Foucher, J.-P., Hilde, T.W.C., Kimura, M., Ling-Yun, C., Marsset, B., Muller, C. and Stephan, J.-F., 1987, Back arc extension in the Okinawa Trough, *Journal of Geophysical Research (Solid Earth)*, vol. 92, 14,041-14,063.

Thompson, G., Humphris, S. E., Schroeder, B., Sulanowska, M. and Rona, P. A., 1988, Active vents and massive sulfides at 26°N (TAG) and 23°N (SNAKEPIT) on the Mid-Atrantic Ridge. *Canadian Mineralogist*, vol. 26, 679-711.

Younger, P. L., Banwart, S. A. and Hedin, R. S., 2002, Mine Water. Kluwer Academic Pub., 452p.

*: in Japanese with English abstract

**: in Japanese

日本語要旨：

沖縄トラフ、伊是名海穴、Hakurei サイトにおける海底熱水沈殿物の風化過程

初川悠[1]・中島和夫[2]・湯口貴史[3]

1: 山形大学大学院理工学研究科　〒990-8560　山形市小白川町 1-4-12

2：（株）ASN　〒989-3204 仙台市青葉区南吉成 6-6-3　LABO･CITY 仙台 1F

3：山形大学理学部　〒990-8560　山形市小白川町 1-4-12

中部沖縄トラフ伊是名海穴の Hakurei サイトにおいて，北部マウンドと南部マウンドの 2 カ所の活性熱水ベントサイトが近年発見された．この 2 つのマウンドから 5 つのサンプルについて顕微鏡観察，XRD，EPMA を用いて鉱物の沈殿と酸化分解作用について検討した．北部マウンドのサンプルには初生鉱物として重晶石，閃亜鉛鉱，磁硫鉄鉱，黄鉄鉱，方鉛鉱，濃紅銀鉱が観察され，一方南部マウンドのサンプルには重晶石，閃亜鉛鉱，黄鉄鉱，方鉛鉱，ヨルダン鉱，ジオクロン鉱，方キューバ鉱が含まれていた．2 つのマウンドの最も顕著な違いは，北部マウンドでは磁硫鉄鉱が晶出するのに対し，南部マウンドでは鉄の硫化物として黄鉄鉱のみ産することである．北部マウンドでは磁硫鉄鉱は水酸化鉄と自然硫黄に分解し，方鉛鉱は硫酸鉛鉱に変化していた．一方、南部マウンドでは Fe 硫化物として黄鉄鉱のみが存在し、それが水酸化鉄に変化し，方鉛鉱はミメット鉱と白鉛鉱に変化していた．

北部マウンドは厚い堆積物に覆われるカルデラ底部に位置しているため，還元的になり pH の低下をもたらす．一方南部マウンドはカルデラ壁に位置し，強い酸化作用によって風化分解が進む．最終的には海底に露出した鉱石のすべての鉱物と沈殿物はその表面から数～数十 cm が分解し，As や Pb，S などの有毒元素が海水へ溶解する．